



Universiteit  
Leiden  
The Netherlands

## **Fundamental Methods to Measure the Orbital Angular Momentum of Light**

Berkhout, G.C.G.

### **Citation**

Berkhout, G. C. G. (2011, September 20). *Fundamental Methods to Measure the Orbital Angular Momentum of Light*. *Casimir PhD Series*. Retrieved from <https://hdl.handle.net/1887/17842>

Version: Not Applicable (or Unknown)

License: [Leiden University Non-exclusive license](#)

Downloaded from: <https://hdl.handle.net/1887/17842>

**Note:** To cite this publication please use the final published version (if applicable).

## Using a multipoint interferometer to measure the orbital angular momentum of light

Recently it was shown that the orbital angular momentum of light can be measured using a multipoint interferometer, a system in which the light from several point measurements is interferometrically combined. This system has important applications in optics but could also be employed to detect astrophysical orbital angular momentum. Until now, the response of a multipoint interferometer to an on-axis, normally incident Laguerre-Gaussian beam has been studied by visual inspection. In this paper we present an algorithm to determine the orbital angular momentum of the impinging beam from the obtained interference patterns. Using this algorithm we extend our study to general optical vortices and a superposition of optical vortices.

G. C. G. Berkhout and M. W. Beijersbergen, *Using a multipoint interferometer to measure the orbital angular momentum of light in astrophysics*, *Journal of Optics A: Pure and Applied Optics* **11**, 094021 (2009).

### 3.1 Introduction

Since its discovery, the orbital angular momentum (OAM) of light has been studied intensively [1, 25]. The fact that light carries angular momentum that, under given circumstances, can be separated into spin and orbital angular momentum is nowadays well known. Recently the possibility that light from astronomical sources possesses OAM was suggested [11, 26]. Detection of this OAM may have interesting implications for astrophysics, since it is known that the OAM of light can be transferred to small particles or atoms (for a recent review, see [25]). A method for detecting OAM in low-frequency radio beams has been proposed recently [12]. Since this method relies on a coherent measurement of the local field vector it cannot be applied to optical wavelengths. In this paper we describe the details of the method that was proposed in [27], based on a so-called multipoint interferometer. The main advantage of this method lies in the fact that it relies on only a finite number of point measurements, making it possible to measure OAM on, in principle, arbitrarily large length scales.

The simplest class of light fields carrying OAM are the so-called optical vortices. A general optical vortex has a complex field amplitude of the form  $\propto \exp(i\ell\phi)$ , resulting in a phase singularity at its centre. At the position of this phase singularity, the intensity drops to zero. As one makes a full turn around the singularity in counterclockwise fashion, the phase increases by  $2\pi\ell$ , where  $\ell$  is the vorticity. Away from the singularity the intensity increases until, for an isolated optical vortex, it consequently drops outside a bright ring of radius proportional to  $\ell$ . The exact form of the intensity profile depends on the origin and propagation of the optical vortex and the presence of other optical vortices. Optical vortices can be created, for example, using a spiral phase plate [5] or a fork hologram [6, 7], but they also occur in more generic fields, such as in speckle patterns [8, 28].

Several methods exist to detect optical vortices. A method that is often used is interfering the optical vortex with a flat wave front. The resulting interference pattern reveals information on the vorticity, the position and the anisotropy of the optical vortex [8]. One can also convert an optical vortex to a Gaussian beam using holographic techniques and detect its intensity using a monomode fibre or pinhole [29]. Both methods require the coverage of an extended region around the optical vortex in order to detect the vorticity.

So far no quantitative analyses of the expected optical vortices from astronomical sources have been presented. The only reasonable assumption one can make is that the associated intensity profile will fluctuate on large scales due to the large propagation distances of the light coming from these sources. It will therefore be virtually impossible to cover a sufficient part of the intensity profile using a single detector, making it impossible to measure the vorticity using interference with a flat wave front. This is illustrated by figure 3.1. One can place the detector near the centre of the optical vortex where the phase varies rapidly, but the amplitude is very low. Alternatively one can place the detector in regions of higher intensity, but hardly any phase change is present there. In a

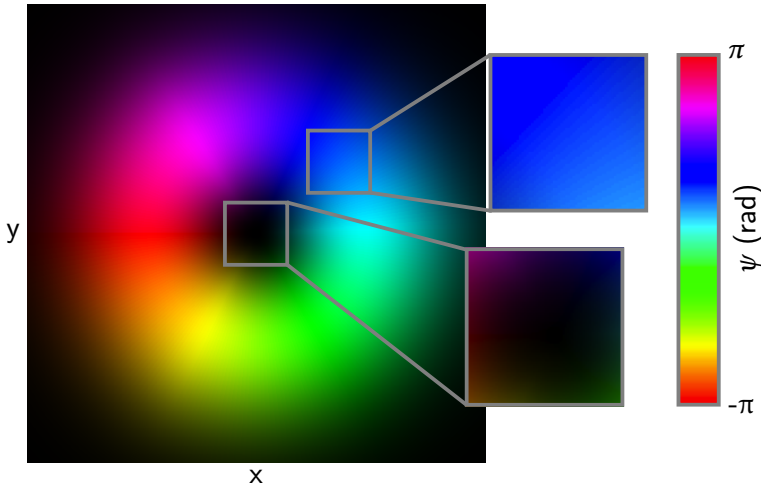


Figure 3.1: A Laguerre-Gaussian  $\ell = 1$  beam (see text for details). Colours indicate phase, while intensity shows amplitude. This figure shows the intrinsic difficulty in measuring the orbital angular momentum of light if only a small part of the beam can be covered using a single detector (shown as grey squares). In the centre there is hardly any intensity, while in the outer parts there is hardly any phase change.

previous paper [27] we discussed an interferometric method based on a so-called multipoint interferometer, where the light of several points, roughly separated by the typical length scale of the intensity fluctuations around the optical vortex, is interferometrically combined. From the resulting interference patterns the vorticity of the impinging vortex can be determined. We experimentally realised the multipoint interferometer by a multi-pinhole interferometer, where we used the diffraction of the light at the pinholes to overlap the light from the different points. Theory and experiment using laser beams prove to be in excellent agreement.

It is possible to scale a multipoint interferometer to, in principle, arbitrary sizes by replacing the pinholes by telescopes and using beam combiner optics to interferometrically combine the light from the different telescopes. This technique could already be implemented at existing telescope arrays, where one has to take into account the non-circular arrangement of the telescopes.

A convenient basis for describing a light beam possessing OAM are the Laguerre-Gaussian beams which have a complex field amplitude given by

$$u_{p\ell}(r, \phi, z) \propto r^\ell L_p^\ell \left( \frac{2r^2}{\tau w^2} \right) \exp \left( -\frac{r^2}{\tau w^2} \right) \exp(-i\ell\phi), \quad (3.1)$$

where  $\tau w$  is the waist size of the beam,  $L_p^\ell(2r^2/\tau w^2)$  is the associated Laguerre polynomial,  $p$  is the radial mode index and  $\ell$  is the vorticity.

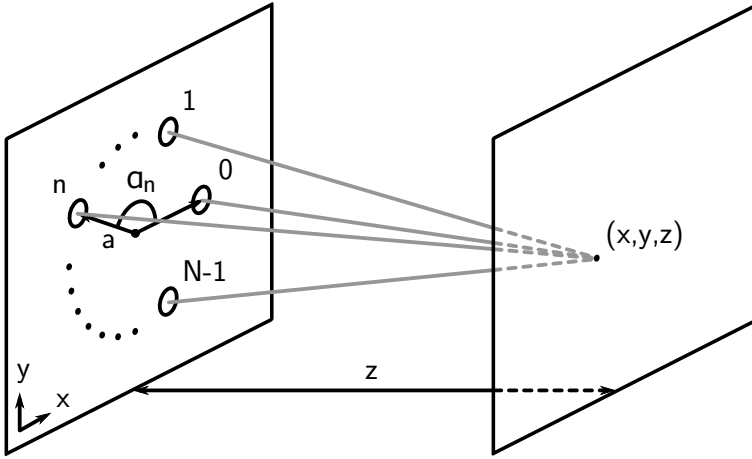


Figure 3.2: Geometry and notation of a generic multipoint interferometer consisting of  $N$  points, uniformly distributed over a circle of radius  $a$  in the  $xy$  plane. The points are indicated by open dots and the angular coordinate of the  $n$ -th point is  $\alpha_n = 2\pi n/N$ .

A general multipoint interferometer consists of  $N$  points, uniformly distributed over a circle of radius  $a$  as shown in figure 3.2. The azimuthal angle of each point is given by  $\alpha_n = 2\pi n/N$ . The far-field interference pattern behind a general multipoint interferometer is given by the Fourier transform of the field distribution in the aperture plane. In the case of an on-axis, normally incident Laguerre-Gaussian beam, the interference pattern is given by

$$I_\ell^N(x, y, z) \propto \left| \sum_{n=0}^{N-1} \exp(-i\ell\alpha_n) \exp\left(i\frac{ka}{z}(x \cos \alpha_n + y \sin \alpha_n)\right) \right|^2. \quad (3.2)$$

Results of this equation are shown in [27] and in figures 3.3 and 3.4.

In any real system the points will be replaced by apertures and the observed interference pattern will be convoluted by the diffraction pattern of an individual aperture. As long as the diameter of the aperture is small compared to the separation of the apertures, the interference pattern can be observed in the central lobe of the diffraction pattern.

Equation 3.2 gives the interesting result that the interference pattern behind a multipoint interferometer of  $N$  points is the same for an impinging beam with  $\ell = m$  and  $\ell' = m + N$  for  $N \geq 4$ . This effect can be explained by comparing the phases of the impinging fields at the different points for both  $\ell$  states. The number of distinguishable  $\ell$  states is therefore equal to  $N$  and the observed patterns are periodic in  $\ell$ .

It is also observed that the patterns for  $\ell = -|m|$  and  $\ell = |m|$  are the same but mirrored in the  $x$  axis. For an even number of points  $N$ , the observed interference patterns are symmetric about the  $x$  axis and it is in this case impossible to distinguish between  $\ell =$

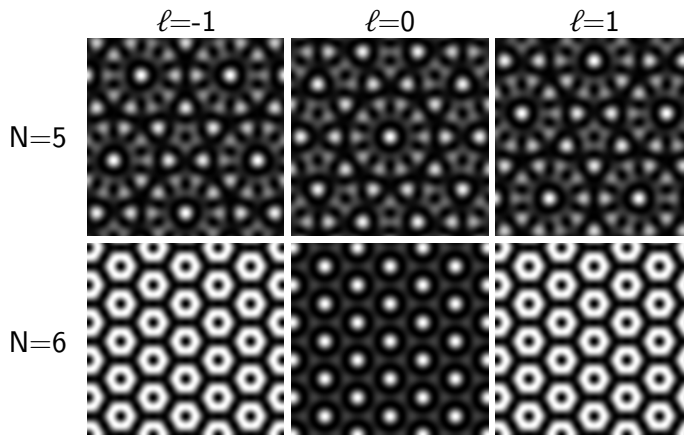


Figure 3.3: Far-field intensity patterns behind an multipoint interferometer of  $N$  points illuminated by a Laguerre-Gaussian beam with vorticity  $\ell$ , calculated from equation 3.2. The patterns for  $\ell = -|\mathcal{m}_z|$  and  $\ell = |\mathcal{m}_z|$  are mirrored in the  $x$  axis. For an odd number of points  $N$ , one can differentiate between the patterns for even and odd values of  $\ell$ ; for even  $N$  one cannot.

$-|\mathcal{m}_z|$  and  $\ell = |\mathcal{m}_z|$ , reducing the number of distinguishable  $\ell$  states to  $N/2 + 1$ . Figure 3.3 shows this behaviour for  $N = 5$  and  $N = 6$ . This behaviour is already explained in [27], but is shown here for the sake of completeness.

In a real application one has to take these effects into account in selecting the number of points. It is for instance known that in all observed speckle patterns only optical vortices with  $\ell = -1$  and  $\ell = 1$  occur [8]. In this case a multipoint interferometer with  $N = 5$  would suffice.

For a large number of points  $N$ , the multipoint interferometer converges to an annular aperture and the resulting interference pattern is described by the well know Bessel function. The order of the Bessel function depends on the  $l$  state of the impinging Laguerre-Gaussian beam since

$$\lim_{N \rightarrow \infty} I_\ell^N(x, y, z) \propto \mathcal{J}_{|\ell|} \left( \frac{kr}{z} \right). \quad (3.3)$$

In this limit one cannot distinguish between clockwise and counterclockwise vortices of the same vorticity. Figure 3.4 illustrates that the convergence can already be seen for relatively small number of points, in this case  $N = 16$ .

So far we have only considered the response to an on-axis, normally incident Laguerre-Gaussian beams, studied by visual inspection. In this paper we will describe an algorithm that can be used to determine the vorticity based on the interference patterns. Using this algorithm we will generalise our findings to general optical vortices.

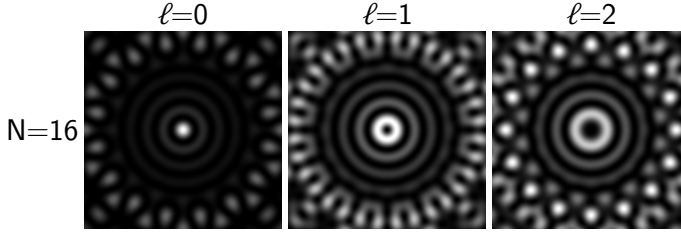


Figure 3.4: Far-field intensity patterns behind an multipoint interferometer of  $N = 16$  points illuminated by a Laguerre-Gaussian beam with vorticity  $\ell$ . The intensity patterns hint at the fact that the patterns converge to a Bessel function in the limit that  $N \rightarrow \infty$  as described by equation 3.3.

### 3.2 Characterising interference patterns

A general optical field can be decomposed on a bases of Laguerre-Gaussian beams, see e.g. [30]

$$u(r, \phi, z) \propto \sum_{\ell=-\infty}^{\infty} c_{\ell} u_{p\ell}(r, \phi, z), \quad (3.4)$$

where  $c_{\ell}$  is a weighting coefficient and  $u_{p\ell}(r, \phi, z)$  are the pure Laguerre-Gaussian modes as described by equation 3.1. As it turns out from the simulations, the interference pattern behind a general multipoint interferometer for this general wave front can be described by

$$I^N = \sum_{\ell=m_{\mathcal{L}}}^{N+m_{\mathcal{L}}-1} c_{\ell} I_{\ell}^N, \quad (3.5)$$

where  $m_{\mathcal{L}}$  indicates an arbitrary integer and  $I_{\ell}^N$  are the interference patterns behind a general multipoint interferometer for a pure Laguerre-Gaussian mode as described by equation 3.2. Note that the summation runs over  $N$  terms only since the interference patterns for  $\ell = m_{\mathcal{L}}$  and  $\ell = m_{\mathcal{L}} + N$  are the same and hence we can only distinguish  $N$  different  $c_{\ell}$ . In case  $N$  is even the summation runs over  $N/2 + 1$  terms only.  $m_{\mathcal{L}}$  can be chosen arbitrarily since the interference patterns are periodic in  $\ell$ . The surprising fact is that the intensity patterns form an orthogonal basis for describing the interference patterns.

In practise the weighting constants  $c_{\ell}$  can be found by performing a 2D convolution algorithm to the interference patterns calculated by

$$c_{\ell} = I^N ** I_{\ell}^N(o, o) = \mathcal{F}^{-1} \{ \mathcal{F} \{ I^N \} * \mathcal{F} \{ I_{\ell}^N \} \} (o, o), \quad (3.6)$$

where  $**$  denotes convolution,  $\mathcal{F}$  and  $\mathcal{F}^{-1}$  2D Fourier transform and 2D inverse Fourier transform respectively and  $(o, o)$  the central pixel of the convolution. In the following analyses this algorithm is used to determine the weighting factors  $c_{\ell}$ . This algorithm requires knowledge of the response of a multipoint interferometer, but as can be seen in

equation 3.2 this response is determined by the number of points and the separation of the pinholes only. For any real optical system the diffraction of the light at the apertures has to be taken into account, but as stated above this will only introduce an envelope on the observed interference pattern.

### 3.3 General optical vortices

#### 3.3.1 Tilt

In general the singularity axis of an impinging optical vortex will not coincide with the axis of the multipoint interferometer, which will have an effect on the observed interference patterns. We have studied the effect of a tilt of the optical vortex with respect to the multipoint interferometer.

As can be seen from figure 3.5, a tilt of the impinging optical vortex results in a shift of the observed interference patterns, as is expected since these are far-field interference patterns. In order to determine the vorticity of the optical vortex one first has to shift the pattern to remove the shift introduced by the tilt. This is possible since the centre of the interference pattern is unique for  $N \geq 5$ , except for  $N = 6$ . For  $N = 4$  and  $N = 6$ , the centre of the pattern is not uniquely determined but centring at any of the repeating unit patterns will work in this case. In the case of a real detection system, the observed interference pattern is convoluted by the diffraction pattern of a single aperture, which makes it more difficult to find the centre of the interference pattern. Before applying the algorithm described above, one has to make sure that there are enough periods of the interference pattern in the central lobe of the diffraction pattern.

#### 3.3.2 Displacement

A displacement of the beam with respect to the multipoint interferometer results in a blurring of the observed interference patterns as can be seen in figure 3.6. The displacement is quantified by a vector  $\mathbf{r}_o = (x_o, y_o, o)$ . In order to analyse these blurred patterns we use the algorithm that is described above to determine the coefficients  $c_\ell$ . In the simulations we capture only a finite part of the infinite interference patterns, which introduces a certain amount of error in the values  $c_\ell$ . For consistency with the previous part of this paper, we choose the same pinhole separation as used above. However, we note that the error in the determination of  $c_\ell$  can be minimised by increasing the pinhole separation.

We calculated the normalised overlap with the different modes for a optical vortex that is displaced over  $\mathbf{r}_o = (x_o, o, o)$ . To avoid effects coming from the intensity profile of the optical vortex, we only consider the phase of the optical vortex and set the intensity to be uniform. As explained before the intensity fluctuations for large optical vortices are expected to be on large scales and the intensity between the different points or apertures will not vary much. The results are shown in figure 3.7. As expected, for an on-axis beam, the coefficient  $c_\ell$  equals one for  $\ell = 1$  and is zero elsewhere. As the beam is displaced,

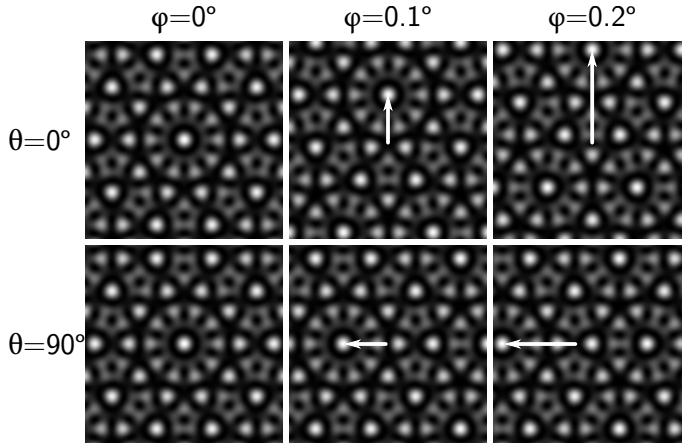


Figure 3.5: Far-field intensity patterns behind a multipoint interferometer of  $N = 5$  illuminated by a Laguerre-Gaussian beam with vorticity  $\ell$ . The propagation axis of the impinging beam is tilted with respect to the normal of the multipoint interferometer over  $\theta$  and  $\phi$ , which are the azimuthal and polar angles respectively. The tilt results in a shift of the observed interference pattern as is indicated by the white arrows.

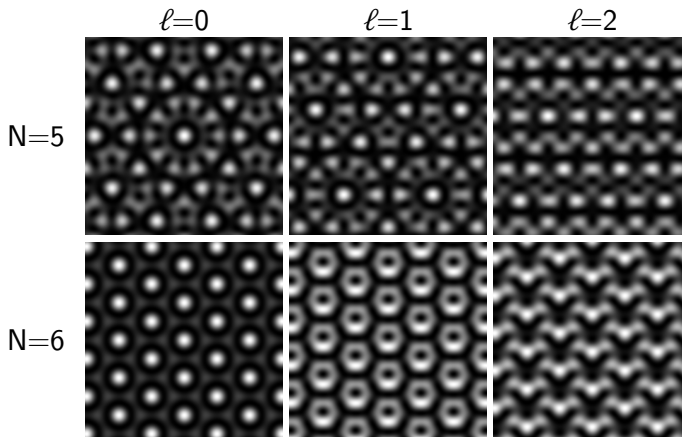


Figure 3.6: Far-field interference patterns behind a multipoint interferometer with  $N = 5$  illuminated by an optical vortex of uniform intensity with its centre displaced over  $\mathbf{r}_0 = (0.5a, 0, 0)$ . The displacement results in a blurring of the interference patterns.

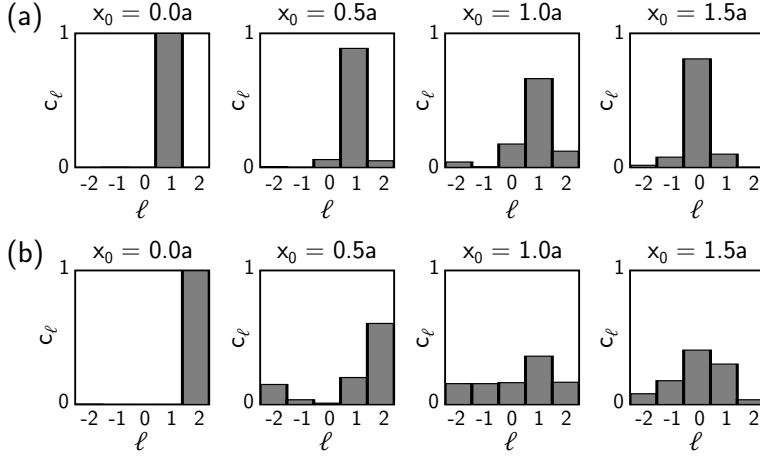


Figure 3.7: (a) Decomposition (see equations 3.5 and 3.6) for a displaced optical vortex with uniform intensity and vorticity  $\ell = 1$ . The position of the singularity is displaced over distance  $\mathbf{r}_o = (x_o, 0, 0)$ . In the limit that the singularity is far from the multipoint interferometer, the wave front that is sensed by the multipoint interferometer becomes essentially flat. (b) Same calculation, but for an optical vortex with  $\ell = 2$ .

the distribution broadens, but still peaks at  $\ell = 1$  of the impinging optical vortex. For even larger displacements there is more and more overlap with the  $\ell = 0$  state. Once the singularity moves out of the circle transcribing the pinholes, the  $\ell = 0$  component dominates. Further simulations show that this switching behaviour happens very fast. The fact that the distribution converges to a pure  $\ell = 0$  state can intuitively be understood, since the wave front that is sensed by the multipoint interferometer effectively becomes flat as the singularity is far away from the centre of the multipoint interferometer.

For an impinging optical vortex with  $\ell = 2$ , we observe the same behaviour, but in two steps. The resulting interference pattern first shows a strong peak at  $\ell = 1$  mode before it finally converges to an  $\ell = 0$  state. These simulations confirm the fact it is possible to determine the vorticity of an optical vortex as long as the singularity axis is within the circle through the points of the multipoint interferometer.

### 3.3.3 Anisotropic optical vortices

Many optical vortices that occur in more generic systems, for instance speckle patterns, are anisotropic, meaning that the phase does not increase linearly with the azimuthal angle around the phase singularity (see figure 3.8). These anisotropic optical vortices can be described by a set of Stokes parameters, using a single parameter  $\alpha$  to describe the anisotropy [31, 32] where  $0 \leq \alpha \leq \pi$ . We analysed the performance of the multipoint interferometer impinged by an anisotropic optical vortex for varying  $\alpha$  in terms of its decomposition on the different pure modes. In the simulations we used the same pa-

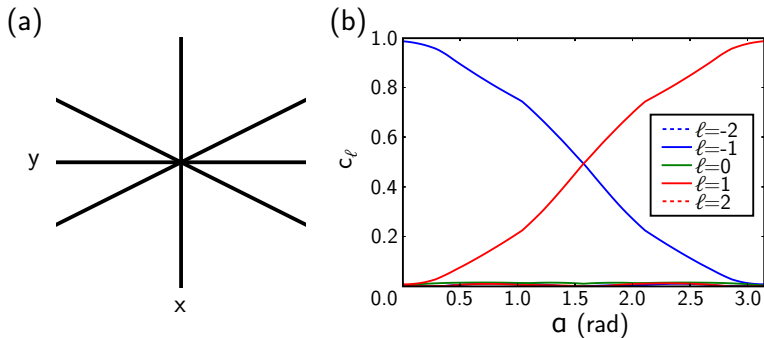


Figure 3.8: (a) Phase profile of an anisotropic optical vortex. The color coding is the same as in figure 3.1. Lines indicate phase contours separated by  $\pi/4$ . (b) Mode decomposition as a function of  $\alpha$  obtained by applying the algorithm as described by equation 3.6.

rameters as above and again only consider the phase of the optical vortex and assume a uniform intensity. One can see that the system is able to determine the vorticity of the impinging beam, except in the region around  $\alpha = \pi/2$  where the vortex reduces to an edge dislocation and the vorticity is not defined. The width of the region in which the vorticity is determined is dependent on the experimental error and depends on the real application. As before we note that the error is strongly dependent on the distance between the points, and that the simulations are not optimised for reducing the error. One can see that the vortex changes sign as the anisotropy goes through  $\alpha = \pi/2$  since the orientation of the zero field lines of the real and imaginary part changes sign here.

### 3.3.4 Superposition of optical vortices

It is possible to generate a superposition of Laguerre-Gaussian beams using, for instance, a fork hologram [29, 33]. For communication purposes it would be interesting to be able to decompose this superposition on a basis of pure modes. A general superposition is described by equation 3.5. As described above one can use only  $N$  different pure modes when using a multipoint interferometer of  $N$  points. Figure 3.9 (a) shows the interference pattern for behind a multipoint interferometer with  $N = 5$  for a randomly chosen set of superposition coefficients shown in figure 3.9 (b) as input. Figure 3.9 (b) also shows the output coefficients  $c_\ell$  determined using the algorithm described above. The difference between the input and output values is caused by fact that there is some error in the output coefficients  $c_\ell$  because of the fact that only a finite part of the interference pattern is captured. This can be improved by capturing a larger part of the pattern, for instance by increasing the separation between the points in the multipoint interferometer. This parameter has not been optimised in these simulations.

These simulations show that it is possible to decompose a superposition of optical vortices with different  $\ell$  modes onto a basis of pure  $\ell$  modes using a multipoint interfer-

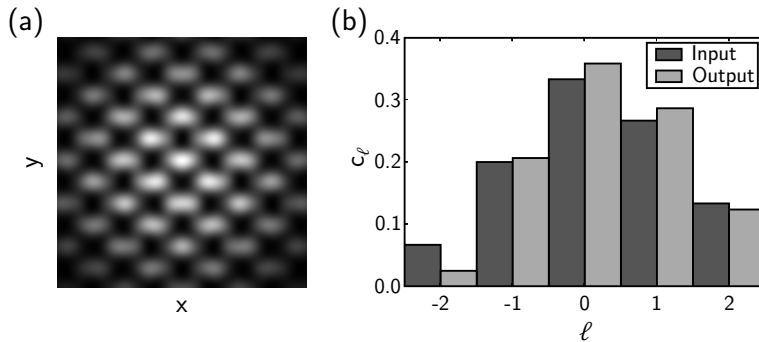


Figure 3.9: (a) Far-field interference pattern behind a multipoint interferometer with  $N = 5$  illuminated by a randomly chosen superposition of Laguerre-Gaussian modes. (b) Input randomly chosen superposition coefficients  $c_\ell$  versus output coefficients as determined by using the method described above.

ometer. It requires however several Fourier transforms to perform this decomposition, which cost valuable computation time, making it not very useful for fast communication purposes as opposed to the method proposed by [33] that returns the coefficients  $c_\ell$  without calculation. The multipoint interferometer can however be useful in cases where the beam is strongly diverging, which might occur in long range communication.

### 3.4 Conclusion

We described an algorithm to characterise the response of a multipoint interferometer and used it to study this response in the case of a general optical vortex and a superposition of optical vortices. This showed that in most cases it is possible to measure the vorticity of the optical vortex. We also showed that a multipoint interferometer can be used to decompose a superposition of Laguerre-Gaussian modes, which is potentially useful for application in free space communication, albeit that the analysis is time consuming. We conclude that a multipoint interferometer is a useful tool for measuring the vorticity of a general vortex of, in principle, arbitrary sizes as are expected to be associated with OAM in astrophysics.

---